

RESEARCH

Open Access



# Chronic kidney disease promotes cerebral microhemorrhage formation

Chuo Fang<sup>1</sup>, Wei Ling Lau<sup>2</sup>, Jiahong Sun<sup>3</sup>, Rudy Chang<sup>3</sup>, Adrian Vallejo<sup>1</sup>, Donghy Lee<sup>1</sup>, Jihua Liu<sup>4</sup>, Han Liu<sup>2</sup>, Yu-Han Hung<sup>1</sup>, Yitong Zhao<sup>2</sup>, Annlia Paganini-Hill<sup>1</sup>, Rachita K. Sumbria<sup>1,3</sup>, David H. Cribbs<sup>4</sup> and Mark Fisher<sup>1,5,6\*</sup>

## Abstract

**Background** Chronic kidney disease (CKD) is increasingly recognized as a stroke risk factor, but its exact relationship with cerebrovascular disease is not well-understood. We investigated the development of cerebral small vessel disease using in vivo and in vitro models of CKD.

**Methods** CKD was produced in aged C57BL/6J mice using an adenine-induced tubulointerstitial nephritis model. We analyzed brain histology using Prussian blue staining to examine formation of cerebral microhemorrhage (CMH), the hemorrhagic component of small vessel disease and the neuropathological substrate of MRI-demonstrable cerebral microbleeds. In cell culture studies, we examined effects of serum from healthy or CKD patients and gut-derived uremic toxins on brain microvascular endothelial barrier.

**Results** CKD was induced in aged C57BL/6J mice with significant increases in both serum creatinine and cystatin C levels ( $p < 0.0001$ ) without elevation of systolic or diastolic blood pressure. CMH was significantly increased and positively correlated with serum creatinine level (Spearman  $r = 0.37$ ,  $p < 0.01$ ). Moreover, CKD significantly increased Iba-1-positive immunoreactivity by 51% ( $p < 0.001$ ), induced a phenotypic switch from resting to activated microglia, and enhanced fibrinogen extravasation across the blood–brain barrier (BBB) by 34% ( $p < 0.05$ ). On analysis stratified by sex, the increase in CMH number was more pronounced in male mice and this correlated with greater creatinine elevation in male compared with female mice. Microglial depletion with PLX3397 diet significantly decreased CMH formation in CKD mice without affecting serum creatinine levels. Incubation of CKD serum significantly reduced transendothelial electrical resistance (TEER) ( $p < 0.01$ ) and increased sodium fluorescein permeability ( $p < 0.05$ ) across the endothelial monolayer. Uremic toxins (i.e., indoxyl sulfate, p-cresyl sulfate, and trimethylamine-N-oxide) in combination with urea and lipopolysaccharide induced a marked drop in TEER compared with the control group ( $p < 0.0001$ ).

**Conclusions** CKD promotes the development of CMH in aged mice independent of blood pressure but directly proportional to the degree of renal impairment. These effects of CKD are likely mediated in part by microglia and are associated with BBB impairment. The latter is likely related to gut-derived bacteria-dependent toxins classically associated with CKD. Overall, these findings demonstrate an important role of CKD in the development of cerebral small vessel disease.

**Keywords** Cerebral microhemorrhages/microbleeds, Aging, Chronic kidney disease, Microglial activation, Brain endothelial cells, Blood–brain barrier, Uremic toxins

\*Correspondence:

Mark Fisher

mfisher@hs.uci.edu

Full list of author information is available at the end of the article



© The Author(s) 2023. **Open Access** This article is licensed under a Creative Commons Attribution 4.0 International License, which permits use, sharing, adaptation, distribution and reproduction in any medium or format, as long as you give appropriate credit to the original author(s) and the source, provide a link to the Creative Commons licence, and indicate if changes were made. The images or other third party material in this article are included in the article's Creative Commons licence, unless indicated otherwise in a credit line to the material. If material is not included in the article's Creative Commons licence and your intended use is not permitted by statutory regulation or exceeds the permitted use, you will need to obtain permission directly from the copyright holder. To view a copy of this licence, visit <http://creativecommons.org/licenses/by/4.0/>. The Creative Commons Public Domain Dedication waiver (<http://creativecommons.org/publicdomain/zero/1.0/>) applies to the data made available in this article, unless otherwise stated in a credit line to the data.

## Background

Chronic kidney disease (CKD) is a major public health issue that affects 15% of U.S. adults, leading to impaired quality of life [1]. Meta-analysis and systemic review of population-based studies provide strong evidence supporting CKD as an independent risk factor for cerebral small vessel disease and cognitive impairment [2–4]. Notably, end-stage renal disease is associated with a substantially higher risk of both ischemic and hemorrhagic strokes [3] as well as accelerated brain aging and cognitive decline [5], and consequently, higher morbidity and mortality [6]. Postmortem examination of CKD human brains showed an increased prevalence of cerebral small vessel disease and highlighted the frequency of microvascular calcification in those brains [7]. Pathways that promote cerebral small vessel disease in the uremic milieu include loss of calcium/phosphorus homeostasis, blood pressure variability, retention of vascular toxins, and chronic inflammation [8]. Investigations into the relationship between CKD and cerebral small vessel disease subtypes are needed to identify novel prevention and treatment strategies in CKD patients.

Cerebral microhemorrhages (CMH) are the pathological substrate for cerebral microbleeds, which represent focal hemosiderin/iron deposits on MRI and are linked to cognitive impairment and ischemic and hemorrhagic stroke. Given that cerebral microbleeds are strongly age-dependent [9] and are present in up to 50% of hemodialysis patients [10], microbleeds may predict vascular outcomes in CKD patients [11, 12]. However, the relationship between CKD and development of cerebral microbleeds is not well-understood in human studies due to concurrent comorbidities such as diabetes and hypertension that also affect the cerebral microvasculature [7]. In comparison, animal models have the advantage of isolating the effect of CKD from other vascular risk factors and thus can provide insights into the direct relationship between CKD and CMH. We previously described a mouse CKD model with adenine-induced tubulointerstitial nephritis and reported more than two-fold increase in CMH burden during an inflammatory state [13]. We previously showed that aging increased inflammation-induced CMH, likely by microglial activation and blood–brain barrier (BBB) disruption [14]. CKD promotes premature aging by inducing inflammation and oxidative stress via a wide range of risk factors including uremic toxins, dialysis, epigenetic factors, and cellular senescence [15]. However, whether CKD mediates age-related CMH formation and underlying pathogenic mechanisms have remained unclear.

Gut-derived uremic toxins, notably endotoxin (lipopolysaccharide, LPS), indoxyl sulfate (IS), p-cresyl sulfate (PCS), and trimethylamine-N-oxide (TMAO) [16–18],

along with urea [13, 13] can exert deleterious effects on brain microcirculation, neurons, microglia, and astrocytes [19]. Beyond that, uremic toxins can exacerbate systemic and local inflammation [19] that may further enhance the pre-existing CMH burden [14]. Our previous work has shown that uremic toxins in CKD patients reduced transendothelial electrical resistance (TEER) and tight junction proteins of a murine brain endothelial cell monolayer in a dose-dependent manner [13], supporting a mechanistic role of uremic toxins in BBB disruption and the development of CMH. We therefore performed the current study to further investigate the relationship between CKD and CMH development in a mouse model of aging. We also examined the effect of CKD serum and uremic toxins on brain microvascular endothelial cell function *in vitro*. Our results help expand knowledge of brain microvascular consequences of CKD and provide mechanistic insights.

## Materials and methods

### In vivo experiments

#### *Animals and chronic kidney disease model*

Aged (17 months) C57BL/6J female and male mice (National Institute of Aging, Bethesda, MD) were randomly divided into control and CKD groups ( $n = 15$ – $17$  per sex per group). Progressive kidney injury was induced in 17-month-old mice using an adenine-induced tubulointerstitial nephritis model, which is equivalent to CKD development over 4 years in 55-year-old humans [20]. After 1 week of acclimation, mice were placed on a diet containing 0.2% adenine (Sigma-Aldrich, St. Louis, MO, USA; diet manufactured at Dyets Inc., Bethlehem, PA) for 18 days, followed by regular chow for 2 weeks, and then re-exposed to adenine diet for 1 week to maintain CKD. Mice were terminated 2 weeks after the second adenine exposure (Fig. 1A) [13]. Systolic and diastolic blood pressure levels were assessed prior to initial CKD induction (Baseline) and termination (Final) using the non-invasive tail-cuff technique (CODA, Kent Scientific, Torrington, CT, USA) [21]. All experimental procedures followed the NIH Guide for the Care and Use of Laboratory Animals and were approved by the Institutional Animal Care and Use Committee at the University of California, Irvine.

#### *Microglial depletion model*

To investigate the role of microglia in CKD-induced CMH formation, we used a highly selective colony-stimulating factor 1 receptor (CSF1R) inhibitor PLX3397 (pexidartinib, MedChemExpress, New Jersey, USA), which reduces microglia number by up to 99% after 3 weeks of treatment [22]. As shown in Fig. 4A, CKD was induced via 0.2% adenine diet in aged (17 months) C57BL/6J female and male mice as described above. Following the

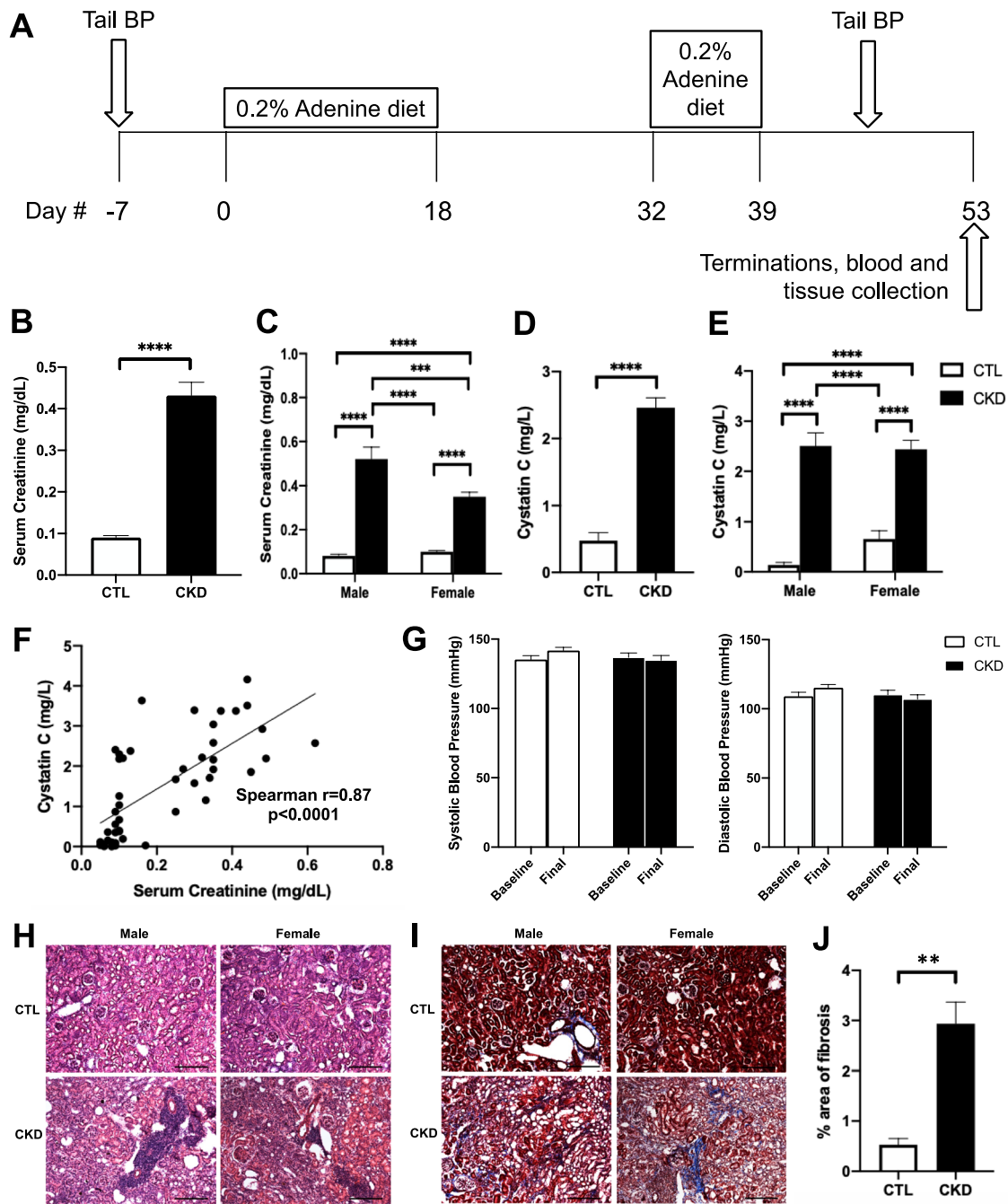


**Fig. 1** Adenine-induced chronic kidney disease (CKD) mouse model. **A** Experimental timeline. Aged (17 months) C57BL/6J mice were placed on a diet containing 0.2% adenine for 18 days, followed by 2 weeks of regular diet, and then re-exposed to 0.2% adenine-containing diet for 1 week to maintain CKD induction. Mice were terminated 2 weeks after the second adenine exposure was completed. **B, C** Mice with adenine-induced CKD showed significantly higher serum creatinine levels (mg/dL) in both males and females compared with control (CTL) mice. **D, E** Serum cystatin C (mg/L) was elevated in CKD animals and **F** correlated closely with serum creatinine. **G** Systolic and diastolic blood pressure (mmHg) were assessed prior to initial CKD induction (Baseline) and termination (Final) using the non-invasive tail-cuff technique. **H** Representative photomicrographs of kidney H&E from CTL and CKD mice. CKD animals demonstrated interstitial inflammation and tubular injury. **I** Representative photomicrographs of kidney Masson's trichrome staining from CTL and CKD animals. CTL mice demonstrated some collagen deposition (blue) around arterioles (normal finding). **J** CKD animals had increased parenchymal fibrosis (blue) consistent with chronic injury. Scale bar = 200  $\mu$ m. Data shown are mean  $\pm$  SEM.  $n = 15-17$  per sex per group. \*\* $p < 0.01$ , \*\*\* $p < 0.001$  and \*\*\*\* $p < 0.0001$

second adenine exposure, mice received regular chow or PLX3397 diet (290 mg/kg, diet manufactured at Dyets Inc., Bethlehem, PA) for 3 weeks prior to mouse terminations. Systolic and diastolic blood pressure levels were assessed as described above.

#### **Tissue collection and blood chemistries**

Mice were euthanized with inhaled isoflurane followed by cardiac perfusion with ice-cold phosphate-buffered saline (PBS) for 5 min. Brains were harvested, fixed overnight in 4% paraformaldehyde (Thermo Fisher Scientific, Cleveland, OH, USA), and passaged through 15% and 30% sucrose solutions prior to storage at  $-70^{\circ}\text{C}$ . Brains were then processed for histological analyses as described previously [14]. Serum samples were collected for creatinine measurements via isotope dilution liquid chromatography with tandem mass spectrometry (LC-MS/MS) at the O'Brien Center Bioanalytical Core (University of Alabama at Birmingham, Birmingham, AL, USA). Serum cystatin C was measured using the mouse ELISA kit (Invitrogen, Carlsbad, CA, USA) per manufacturer's protocol.

#### **Kidney histopathological analysis**

Ten-micron kidney sections were generated using a freezing microtome, stained with hematoxylin and eosin (H&E) or Masson's trichrome, and examined under a photomicroscope (Nikon Eclipse, Japan). An ImageJ macro was used to quantify kidney fibrosis (% area stained blue relative to red on Masson's trichrome) as previously described [23, 24]. Six images of kidney cortex were captured at  $10\times$  magnification from 3 animals per group by an observer blinded to the study groups, and mean % area was calculated per animal.

#### **Detection and quantification of CMH**

The brains were sectioned into  $20\text{-}\mu\text{m}$  or  $40\text{-}\mu\text{m}$  coronal sections with a freezing microtome (Thermo Fisher Scientific, Cleveland, OH, USA). Every seventh section was collected for Prussian blue staining to detect hemosiderin (marker of CMH formation) performed by the Research Services Core (Department of Pathology and Laboratory Medicine at UCI Medical Center). Briefly, sections were stained with freshly prepared 5% potassium hexacyanoferrate trihydrate (Sigma-Aldrich, St. Louis, MO, USA) and 10% hydrochloric acid (Sigma-Aldrich, St. Louis, MO, USA) for 30 min. After rinsing in water, sections were counterstained with nuclear fast red, dehydrated, and coverslipped. To quantify CMH number, CMH were detected and photographed at  $20\times$  magnification with a light microscope by a blinded observer. Whole slide images were scanned to quantify the total area of the brain section. The area of the section was analyzed by a blinded observer using National Institute of Health (NIH)

ImageJ software 1.52. CMH number was then adjusted to total area of the brain section [13].

#### **Immunohistochemistry for neuroinflammation and BBB disruption**

To detect neuroinflammation and BBB disruption, immunohistochemistry for Iba-1 (microglia/macrophages marker), glial fibrillary acidic protein (GFAP, astrocyte marker), and fibrinogen (BBB injury marker) was performed. Briefly,  $20\text{-}\mu\text{m}$  or  $40\text{-}\mu\text{m}$  coronal sections were incubated in 0.3% hydrogen peroxide in  $1\times$  PBS (pH 7.4) for 30 min at room temperature (RT), blocked with PBST containing 1% bovine serum albumin for 2 h at RT. Sections were then incubated overnight at  $4^{\circ}\text{C}$  with rabbit primary antibodies against Iba-1 (1:400 dilution, Wako Chemicals USA, Richmond, VA, USA), GFAP (1:2000 dilution, Abcam, Cambridge, MA, USA), or fibrinogen (1:50 dilution, Abcam, Cambridge, MA, USA). After washing with PBST, sections were incubated with biotinylated anti-rabbit secondary IgG (1:1000 dilution, Jackson ImmunoResearch, West Grove, PA, USA) for 2 h at RT. After washing with PBS, sections were incubated with avidin-biotin-peroxidase (ABC) complex (Vector Laboratories, Burlingame, CA, USA) for 45 min at RT and developed using 3,3'-diaminobenzidine (DAB) (Vector Laboratories, Burlingame, CA, USA). Thirteen images per brain section were acquired from three brain regions (cortex, hippocampus, and thalamus) at  $20\times$  magnification. Quantification of immunoreactive area (expressed as percentage of total analyzed area) was performed by a blinded observer using NIH ImageJ software 1.52, and the average immunoreactive area of three brain regions was calculated [13]. To determine the morphological state of microglia, Iba-1-stained sections were photographed at  $40\times$  magnification, and microglia were categorized into the resting or activated state by a blinded observer. Resting microglia are characterized by long, ramified processes with small cell bodies. In disease states, microglia can be activated and transformed into a phagocytic appearance, exhibiting large, rounded cell bodies with no or few processes [25]. The number of microglia in each state was expressed as the percentage of total microglia.

#### **In vitro experiments**

##### **Human induced pluripotent stem cell (iPSC) culture and differentiation**

iPSC IMR90 clone 4 line (IMR90-4, WiCell, Madison, WI, USA, passage 34–37; Catalog no. WIS-Ci004-B) were differentiated into human brain microvascular endothelial cells (ihBMEC) as described previously [26]. Briefly, IMR90-4 cells were maintained in mTeSR<sup>TM</sup>-Plus medium (STEMCELL Technologies, Vancouver, BC, Canada). For

differentiation, IMR90-4 cells were detached by Accutase (Innovative Cell Technologies, San Diego, CA, USA) and re-plated onto Matrigel-coated 6-well plates at a density of  $2.5 \times 10^4$  cells/cm<sup>2</sup> in mTeSR™-Plus medium supplemented with 10 μM rho-associated protein kinase (ROCK) inhibitor Y-27632 (Selleckchem, Houston, TX, USA) for 3 days. Cell differentiation was induced by treating IMR90-4 cells with Dulbecco's Modified Eagle Medium/Ham's nutrient mixture F-12 (DMEM/Ham's F12) medium (Thermo Fisher, Waltham, MA, USA) supplemented with 6 μM glycogen synthase kinase 3 inhibitor/Wnt activator CHIR99021 (Selleckchem, Houston, TX, USA), 1× minimum essential medium–nonessential amino acids (MEM-NEAA) (Thermo Fisher, Waltham, MA, USA), 0.5× GlutaMAX™ (Thermo Fisher, Waltham, MA, USA), and 0.1 mM β-mercaptoethanol (Sigma-Aldrich, St. Louis, MO, USA) for 1 day. To maintain differentiation, medium was replaced with DMEM/Ham's F12 medium supplemented with 1X MEM-NEAA, 0.5× GlutaMAX™, and 0.1 mM β-mercaptoethanol every 24 h. After 5 days, medium was replaced with human endothelial serum-free medium (hESFM, Invitrogen, Carlsbad, CA, USA) supplemented with 20 ng/mL basic fibroblast growth factor (bFGF), 1× B27 supplement (Thermo Fisher, Waltham, MA, USA) and 10 μM retinoic acid (Sigma-Aldrich, St. Louis, MO, USA) for 3 days for complete differentiation to ihBMEC. Each batch of differentiated ihBMEC was examined for their endothelial phenotype by confirming their cobblestone morphology, expression of endothelial marker von Willebrand factor (vWF), and uptake of acetylated low-density lipoprotein (LDL), as described previously [26].

#### **Murine brain microvascular endothelial cell culture**

bEnd.3 cells (American Type Culture Collection, Manassas, VA, USA; Catalog no. CRL-2299) were cultured in Dulbecco's Modified Eagle's Medium (DMEM, American Type Culture Collection, Manassas, VA, USA) supplemented with 10% fetal bovine serum (FBS, R&D systems, Minneapolis, MN, USA), and 100 μg/mL penicillin/streptomycin (Sigma-Aldrich, St. Louis, MO, USA) at 37 °C (5% CO<sub>2</sub>, 95% air). The endothelial phenotype of the bEnd.3 cells was confirmed by evaluating their cobblestone morphology, expression of endothelial marker vWF, and uptake of acetylated LDL, as described previously [26]. Cells between passage numbers 25–35 were seeded at a density of  $1 \times 10^5$  to  $1 \times 10^6$  cells/cm<sup>2</sup> and grown to confluence on 24-well Transwell inserts (pore size 0.4 μm, Corning Inc., Corning, NY, USA) [26]. Cells were then exposed to uremic toxins for 4 days prior to further experiments. Urea 72 mg/dL, LPS 10 ng/mL, mixture of gut-derived uremic toxins (3Toxins = IS 150 μg/mL + PCS 100 μg/mL + TMAO 1 mg/mL) were tested

alone and in combination. The reference group was cells grown in DMEM with 10% FBS, and mannitol 450 mg/dL was used for an osmotic control group.

#### **TEER measurement**

ihBMEC were replated at a density of  $1 \times 10^6$  cells/cm<sup>2</sup> on 24-well Transwell inserts (pore size 0.4 μm, Corning Inc., Corning, NY, USA) coated with a solution containing 400 μg/mL collagen IV (Sigma-Aldrich, St. Louis, MO, USA) and 100 μg/mL fibronectin (Sigma-Aldrich, St. Louis, MO, USA). To examine the effect of CKD on BBB integrity, ihBMEC were treated with human healthy serum or uremic serum from dialysis patients for 3 days. Based on our prior work in a mouse brain endothelial BBB model in which incubation with CKD serum produced a dose-dependent drop in TEER [13], 15% serum concentration was chosen. Three days of incubation was chosen, because the trophic factors in human serum are sufficient to maintain cell growth and health within 3 days [26]. In a separate experiment, effects of uremic toxins on the bEnd.3 endothelial barrier were assessed by exposing bEnd.3 cells to uremic toxins for 4 days. Integrity of the endothelial monolayer was assessed by measuring TEER using the EVOM2 Epithelial Volt/Ohm Meter and an STX-2 electrode system (World Precision Instruments LLC, Sarasota, FL, USA) every 24 h. TEER values were calculated by subtracting the resistance of cell-free blank Transwells [26]. TEER values for each treatment were expressed as the percentage TEER of the baseline values. Human serum samples from healthy individuals and from end-stage renal disease patients on chronic hemodialysis were obtained from previously banked samples after IRB approval and informed consent.

#### **Tracer permeability measurement**

Tracer permeability across the ihBMEC cell monolayer was assessed after TEER values were stabilized. Sodium fluorescein (5 μg/mL, MW: 376 Da, Sigma-Aldrich, St. Louis, MO, USA) was added to the medium in the apical chamber, and medium in the basolateral chamber was collected after 3 days to determine the passage of sodium fluorescein. The mean fluorescent intensity of sodium fluorescein was measured using a fluorescence plate reader (Molecular Devices, LLC, San Jose, CA, USA) at an excitation/emission wavelength of 460 nm/515 nm. Tracer permeability was expressed as permeability coefficient (cm/s) calculated as described previously [26].

#### **Cell viability assay**

ihBMEC (7500 cells/well) were seeded in 96-well plates (Corning, New York, NY, USA). Cell viability was measured using the Cell Counting Kit-8 (CCK-8) assay according to manufacturer's instructions (Dojindo Molecular

Technologies, Rockville, MD, USA) 3 days after serum treatment initiation. Absorbance was measured at 450 nm using a plate reader (Molecular Devices, LLC, San Jose, CA, USA). Cell viability was expressed as the percentage of ihBMEC controls without serum treatment [26]. bEnd.3 cells ( $3 \times 10^5$  cells/well) were seeded in 6-well plates (Corning, New York, NY, USA) and treated with uremic toxins. Cell viability was measured using trypan blue assay according to manufacturer's instructions (Sigma-Aldrich, St. Louis, MO, USA) 3 days after treatment initiation. Cell viability was expressed as the percentage of total viable cells (unstained) in total cells (stained and unstained).

### Statistical analysis

The data were analyzed by GraphPad Prism 8 (GraphPad Software, Lo Jolla, CA) and SAS version 9.4 (SAS Institute Inc., Cary, NC). Results are presented as means  $\pm$  SEM. Normality tests were performed using D'Agostino-Pearson. Comparison of means was analyzed by Student's *t* test for two independent groups, by two-way ANOVA (e.g., factor 1 treatment CTL/CKD and factor 2 male/female) with post-hoc Sidak-adjusted pairwise comparisons, or by two-way repeated measures ANOVA for timepoint and treatment with post-hoc comparisons. To determine the association between variables, Spearman's correlation tests were performed, and results were presented as correlation coefficient (*r*). *P* value of less than 0.05 was considered statistically significant.

## Results

### Adenine-induced CKD promoted CMH formation in aged C57BL/6 J mice without altering blood pressure levels

In this adenine-induced CKD mouse model, serum levels of creatinine, a biomarker of kidney insufficiency, were increased 3.8-fold in CKD mice ( $0.43 \pm 0.03$  mg/dL vs.  $0.09 \pm 0.01$  mg/dL in controls,  $p < 0.0001$ ) (Fig. 1B). Serum creatinine values were significantly higher in CKD males than CKD females ( $0.52 \pm 0.05$  mg/dL vs.  $0.35 \pm 0.02$  mg/dL,  $p < 0.001$ ) (Fig. 1C). Another marker of kidney injury, cystatin C, was similarly elevated in CKD animals and correlated closely with serum creatinine (Spearman  $r = 0.87$ ,  $p < 0.0001$ ) (Fig. 1D–F). Average serum cystatin C was  $0.14 \pm 0.05$  mg/L and  $0.66 \pm 0.16$  mg/L in control male and female animals; and was  $2.5 \pm 0.26$  mg/L and  $2.44 \pm 0.18$  mg/L in CKD male and female animals (Fig. 1E). H&E staining of kidney sections demonstrated interstitial inflammation and tubular injury in CKD animals (Fig. 1H). On kidney trichrome staining, area of fibrosis was increased 5.5-fold ( $p < 0.01$ ) in CKD animals compared with controls ( $0.5 \pm 0.1$  vs.  $2.9 \pm 0.4\%$  area of fibrosis, respectively) (Fig. 1I, and J). There was no difference in fibrosis

scores between the male and female kidneys from CKD animals (data not shown). This adenine-induced CKD model is non-hypertensive; pre- and post-CKD systolic ( $137 \pm 3$  mmHg to  $135 \pm 3$  mmHg) and diastolic blood pressure ( $110 \pm 3$  mmHg to  $107 \pm 3$  mmHg) remained essentially unchanged (Fig. 1G).

CMH burden was measured by the number of Prussian blue-positive CMH adjusted to total area of the brain section (CMH number per  $\text{cm}^2$ ) (Fig. 2A–E). Prussian blue staining revealed that the average CMH number was significantly higher in CKD mice compared with control mice ( $1.12 \pm 0.10$  per  $\text{cm}^2$  vs.  $0.85 \pm 0.08$  per  $\text{cm}^2$ ,  $p < 0.05$ ) (Fig. 2A, and E). CKD-induced increase in CMH number was more pronounced in males ( $1.26 \pm 0.16$  per  $\text{cm}^2$  vs.  $0.82 \pm 0.12$  per  $\text{cm}^2$  in control males,  $p = 0.11$ ) than in females ( $0.98 \pm 0.13$  per  $\text{cm}^2$  vs.  $0.88 \pm 0.11$  per  $\text{cm}^2$  in control females,  $p = 0.99$ ) (Fig. 2B). CMH number was positively correlated with serum creatinine values in aged mice (Spearman  $r = 0.37$ ,  $p < 0.01$ , Fig. 2C). This positive association was notably greater in males (Spearman  $r = 0.54$ ,  $p < 0.01$ , Fig. 2D), which is in line with a larger increase in serum creatinine in CKD males compared with CKD females. Therefore, CMH burden was significantly increased and associated with the degree of adenine-induced kidney injury.

### CKD induction promoted microglial activation and BBB disruption

To determine if adenine-induced CKD is associated with glial activation and BBB disruption, we performed immunohistochemistry for Iba-1, GFAP, and fibrinogen (Fig. 3A–F). The number and morphology of microglia were quantified and expressed as the percentage of Iba-1 immunoreactive area and percentage of the number of resting and activated microglia as compared to total microglia, respectively. After CKD induction, Iba-1-positive immunoreactivity increased by 51% compared with controls ( $1.84 \pm 0.14$  vs.  $1.22 \pm 0.11\%$  of analyzed brain area,  $p < 0.001$ ) (Fig. 3A, and F), which was accompanied by a small increase in the proportion of activated microglia ( $49.7\% \pm 1.3$  vs.  $45.4\% \pm 1.5$ ,  $p < 0.05$ ) and a corresponding significant decrease in resting microglia (data not shown) (Fig. 3C). GFAP staining was not significantly different between CKD and control mice ( $4.31 \pm 0.62$  vs.  $3.46 \pm 0.3\%$ ). Fibrinogen-positive immunoreactivity was significantly higher by 34% in CKD mice compared with CTL mice ( $1.26 \pm 0.14$  vs.  $0.93 \pm 0.06$ ,  $p < 0.05$ ) (Fig. 3D, and F). CKD significantly increased Iba-1 immunoreactivity in males compared with females ( $p < 0.01$ , Fig. 3B); however, no sex differences were seen with fibrinogen (Fig. 3E). Overall, CKD induction promoted microglial activation and BBB disruption in aged mice, with changes

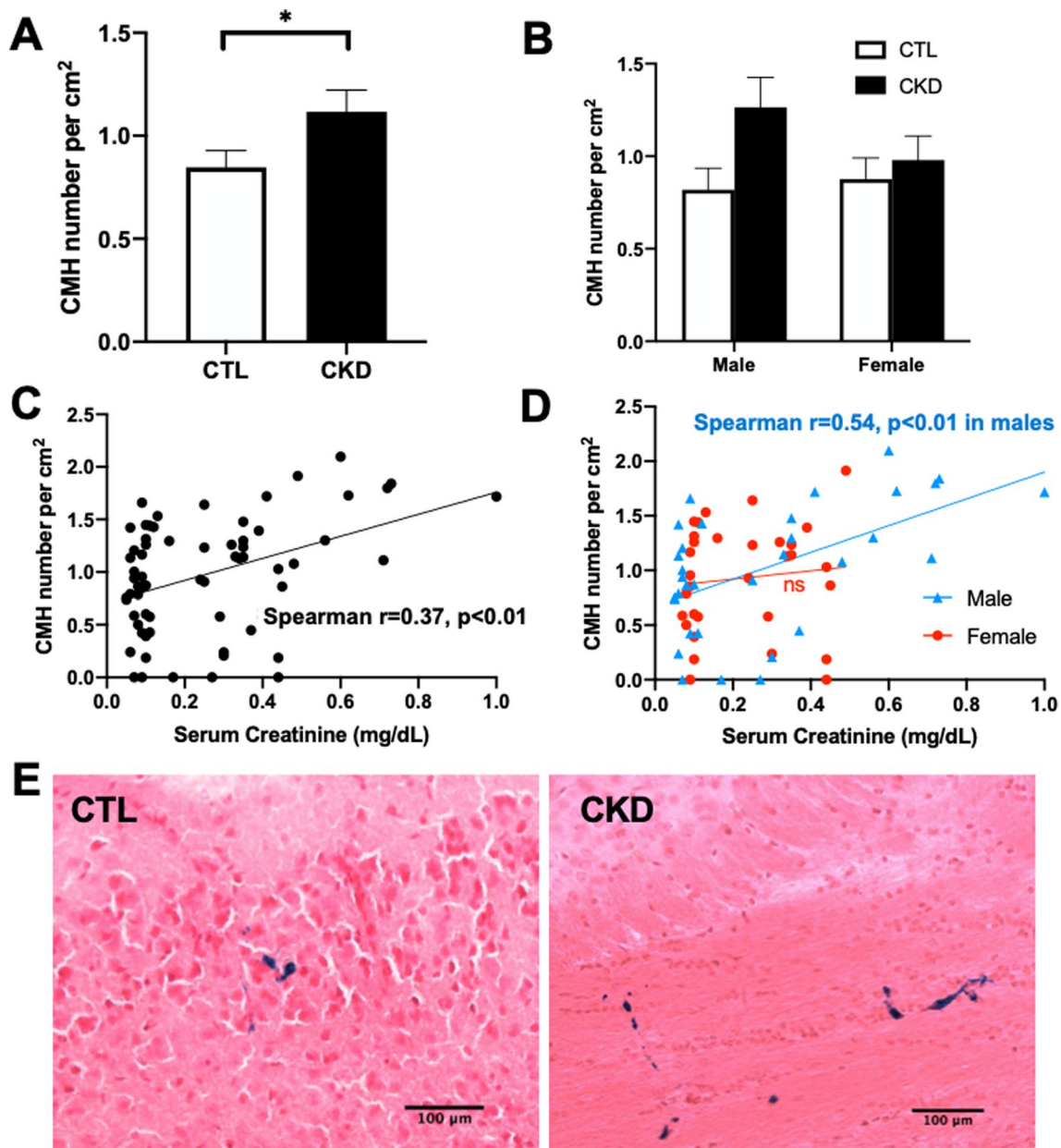


**Fig. 2** CKD induction promoted cerebral microhemorrhages (CMH) formation. **A, B** Significantly higher CMH number, expressed as Prussian blue-positive CMH, in CKD mice compared with CTL mice. **C, D** Prussian blue positivity was positively correlated (Spearman correlation) with serum creatinine values. **E** Representative images of Prussian blue-positive lesions in the subcortex from CTL and CKD mice, indicating CMH burden. Scale bar = 100  $\mu$ m. Data shown are mean  $\pm$  SEM.  $n = 15-17$  per sex per group. \* $p < 0.05$

being more pronounced in CKD males than CKD females.

**Microglial depletion with PLX3397 diet significantly decreased CMH in CKD mice**

We examined the mechanistic link between microglial activation and CMH formation in CKD using PLX3397 diet, which allows for microglial depletion during CMH

formation post-CKD induction. As expected, mice with adenine-induced CKD showed significantly higher serum creatinine levels (Fig. 4B) and CMH number compared with control mice (Fig. 4E, and F). Immunostaining for Iba-1 showed marked decrease in Iba-1 immunoreactive area ( $p < 0.0001$ ) in the mouse brains after 3 weeks of PLX3397 diet (Fig. 4C, and D). Microglial depletion with PLX3397 significantly reduced

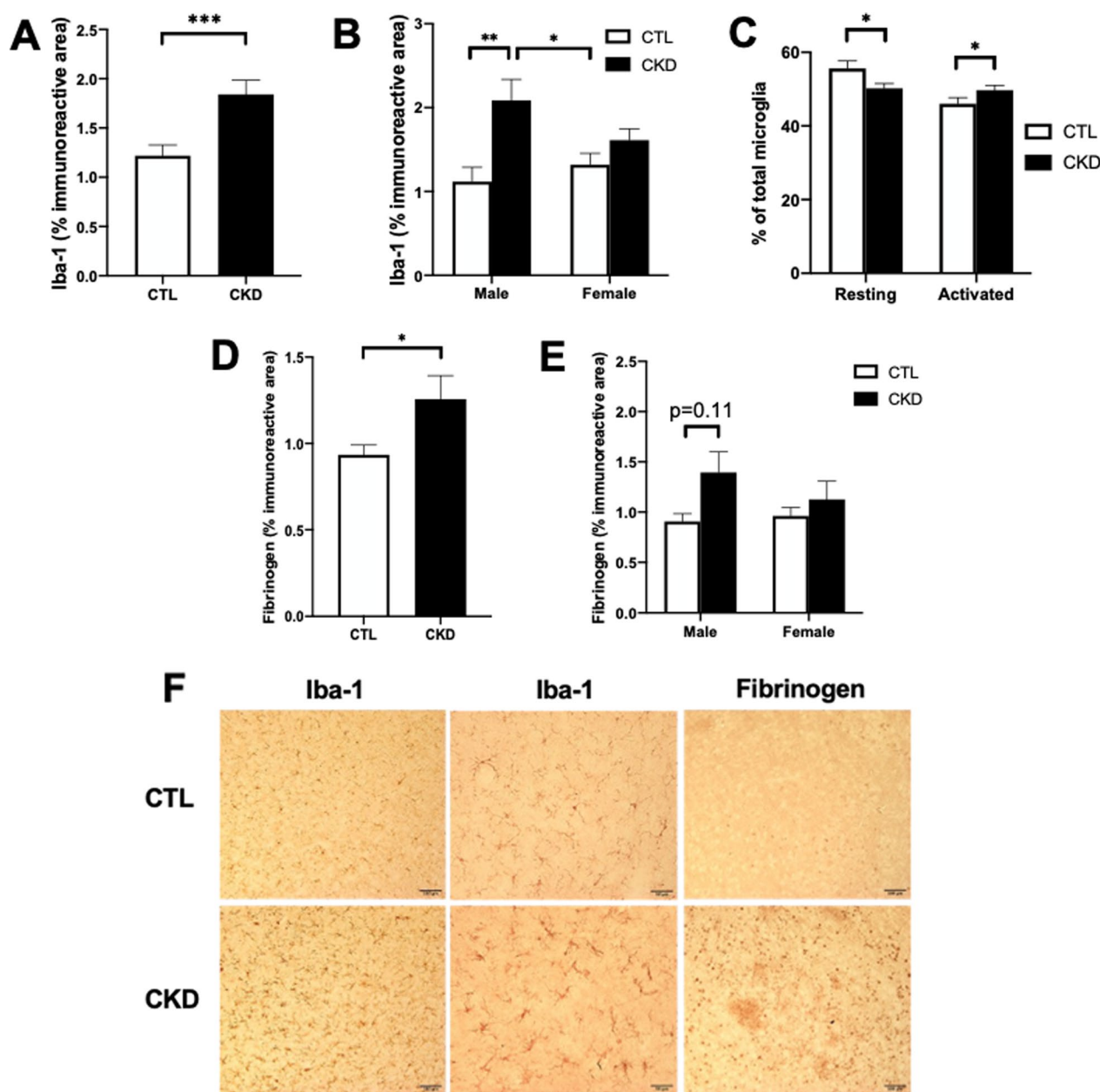


**Fig. 3** CKD induction promoted microglial activation and blood–brain barrier (BBB) disruption. **A, B** Significantly higher Iba-1 immunoreactivity, expressed as % of Iba-1 immunoreactive area, in CKD mice compared with CTL mice. **C** Number of microglia within the two states (resting and activated) expressed as a proportion of the total number of microglia was quantified. CKD mice showed decreased number of resting microglia and increased number of activated microglia compared with CTL mice. **D, E** Fibrinogen immunoreactivity, expressed as % of immunoreactive area, was significantly higher in CKD mice compared with CTL mice. **F** Representative immunohistochemical images of Iba-1 (left: 20× objective, scale bar = 100 μm; middle: 40× objective, scale bar = 50 μm) and fibrinogen (right: 20× objective, scale bar = 100 μm) in the thalamus. Data shown are mean ± SEM. *n* = 15–17 per sex per group. \**p* < 0.05, \*\**p* < 0.01 and \*\*\**p* < 0.001

CMH formation in CKD mice from  $1.92 \pm 0.12$  per  $\text{cm}^2$  to  $1.55 \pm 0.11$  per  $\text{cm}^2$  ( $p < 0.05$ ) (Fig. 4E, and F). No significant differences were observed for systolic and diastolic blood pressure with and without the PLX3397 diet (data not shown).

#### Serum-derived factors in CKD disrupted BBB integrity of the ihBMEC monolayer

To compare effects of healthy and CKD serum on paracellular passage across the ihBMEC monolayer, ihBMEC were treated with serum from either healthy or dialysis patient donors. TEER values showed some initial increase

with both control and CKD serum and plateaued after 2 days of incubation. Following 3 days of incubation, TEER was significantly lower in the CKD serum group ( $157 \pm 8.9\%$  vs.  $195 \pm 7\%$  in the healthy serum group, relative to baseline TEER values;  $p = 0.01$ ) (Fig. 5A). The passive permeability of the brain endothelial monolayer was also assessed. Permeability coefficients of sodium fluorescein were  $1.8 \pm 0.5 \times 10^{-7}$  and  $3.9 \pm 0.6 \times 10^{-7}$  cm/s in cells treated with healthy and CKD serum, respectively, i.e., incubation of ihBMEC with CKD serum doubled the passage of sodium fluorescein ( $p < 0.05$ ) across the monolayer (Fig. 5B). ihBMEC viability, shown as the percentage of control cells without serum treatment, was not affected (Fig. 5C).

#### Gut-derived uremic toxins aggravated urea/LPS-induced bEnd.3 endothelial barrier dysfunction

Effects of uremic toxins on the bEnd.3 endothelial barrier were assessed by TEER measurements from day 0 (baseline) to day 4 (Fig. 5D). TEER values were significantly lower in the 3Toxins+Urea+LPS group compared with the control group. After 4 days of incubation, TEER was significantly lower in the Urea+LPS ( $121 \pm 4.74\%$ ,  $p < 0.01$ ), 3Toxins+LPS ( $122 \pm 3.83\%$ ,  $p < 0.05$ ), and 3Toxins+Urea+LPS group ( $103 \pm 2.38\%$ ,  $p < 0.0001$ ) compared with the control group ( $140 \pm 2.48\%$ ) (Fig. 5D). bEnd.3 cell viability assessed by trypan blue exclusion was equivalent across groups (Fig. 5E).

#### Discussion

In this study, adenine-induced CKD promoted the development of CMH in aged C57BL/6J mice without altering blood pressure levels. CMH number and serum creatinine values were significantly correlated, indicating that the extent of CMH development was directly proportional to degree of renal insufficiency. CKD mice exhibited greater microglial area, a phenotypic switch from resting to activated microglia, and elevated fibrinogen extravasation compared with control mice, indicating CKD-induced microglial activation and BBB disruption in this model. Furthermore, microglial depletion with PLX3397 diet significantly decreased CMH formation in aged CKD mice without affecting serum creatinine levels. We also conducted mechanistic studies using

both human and murine in vitro brain microvascular endothelial models. Our results showed that serum-derived factors in CKD disrupted the ihBMEC monolayer by reducing the TEER values of the monolayer and enhancing the passage of sodium fluorescein across the monolayer. Uremic toxins (i.e., IS, PCS, and TMAO) in combination with low-dose urea and LPS induced a marked drop in the TEER of the bEnd.3 cells. Collectively, these findings indicate that CKD provokes microvascular injury, leading to CMH formation in this model.

Investigating the relationship between CKD and CMH development in the clinical setting is challenging due to the presence of comorbidities (e.g., hypertension and diabetes) that can also incur cerebrovascular injury. Elevated blood pressure has been associated with increased CMH burden [21]. In this adenine-induced CKD mouse model, the association of kidney injury with CMH development was independent of blood pressure levels. Therefore, the relationship was examined in a non-hypertensive mouse model of aging and CKD. The increase in the serum biomarker creatinine (Fig. 1B) due to poor renal clearance confirmed impaired kidney function [27], consistent with our previous work with young animals [13]. We previously reported young mice required supplemental injections of LPS to show the full extent of CKD impact on CMH formation [13]. The current study used aged animals, and the impact of CKD was observable without supplemental LPS. This again emphasizes the role of aging in CMH development and may be related to the known heightened microglial reactivity with aging [28]. We showed that CKD enhanced the development of CMH independent of blood pressure, with a greater extent in mice with more severe kidney injury (Fig. 2C). We noted sex difference in CKD-induced CMH development, whereby males showed a more pronounced increase in CMH number compared with female animals (Fig. 2B) in parallel with significantly higher serum creatinine levels (Fig. 1C), and increased microglial activation (Fig. 3B) and fibrinogen extravasation (Fig. 3E) in CKD males than females. These findings suggest that in the CKD model being investigated, aged male mice are more susceptible to adenine-induced kidney injury than the aged females. In accordance with our findings, a number of population-based studies have demonstrated

(See figure on next page.)

**Fig. 4** Microglial depletion with PLX3397 diet significantly decreased CMH in CKD mice. **A** Experimental timeline. To achieve microglial depletion in CKD mice, aged (17 months) C57BL/6J mice were placed on PLX3397 diet (PLX, 290 mg/kg in regular chow) for 3 weeks after completion of the second adenine exposure. **B** Mice with adenine-induced CKD showed significantly higher serum creatinine levels (mg/dL) compared with CTL mice regardless of microglial depletion. **C** Representative images of Iba-1 immunohistochemical staining in the cortex from CTL and CKD mice with or without microglial depletion, showing **D** Iba-1 immunoreactive area was significantly lower in CTL and CKD mice after microglial depletion. **E** Representative images of Prussian blue-positive lesions in the subcortex from CTL and CKD mice with or without microglial depletion, showing **F** CMH formation in CKD mice was significantly decreased after microglial depletion. Scale bar = 100  $\mu$ m. Data shown are mean  $\pm$  SEM.  $n = 10$  in NonPLX-CTL group, 10 in PLX-CTL group, 36 in NonPLX-CKD group, and 25 in PLX-CKD group. \* $p < 0.05$ , \*\* $p < 0.01$ , \*\*\* $p < 0.001$  and \*\*\*\* $p < 0.0001$

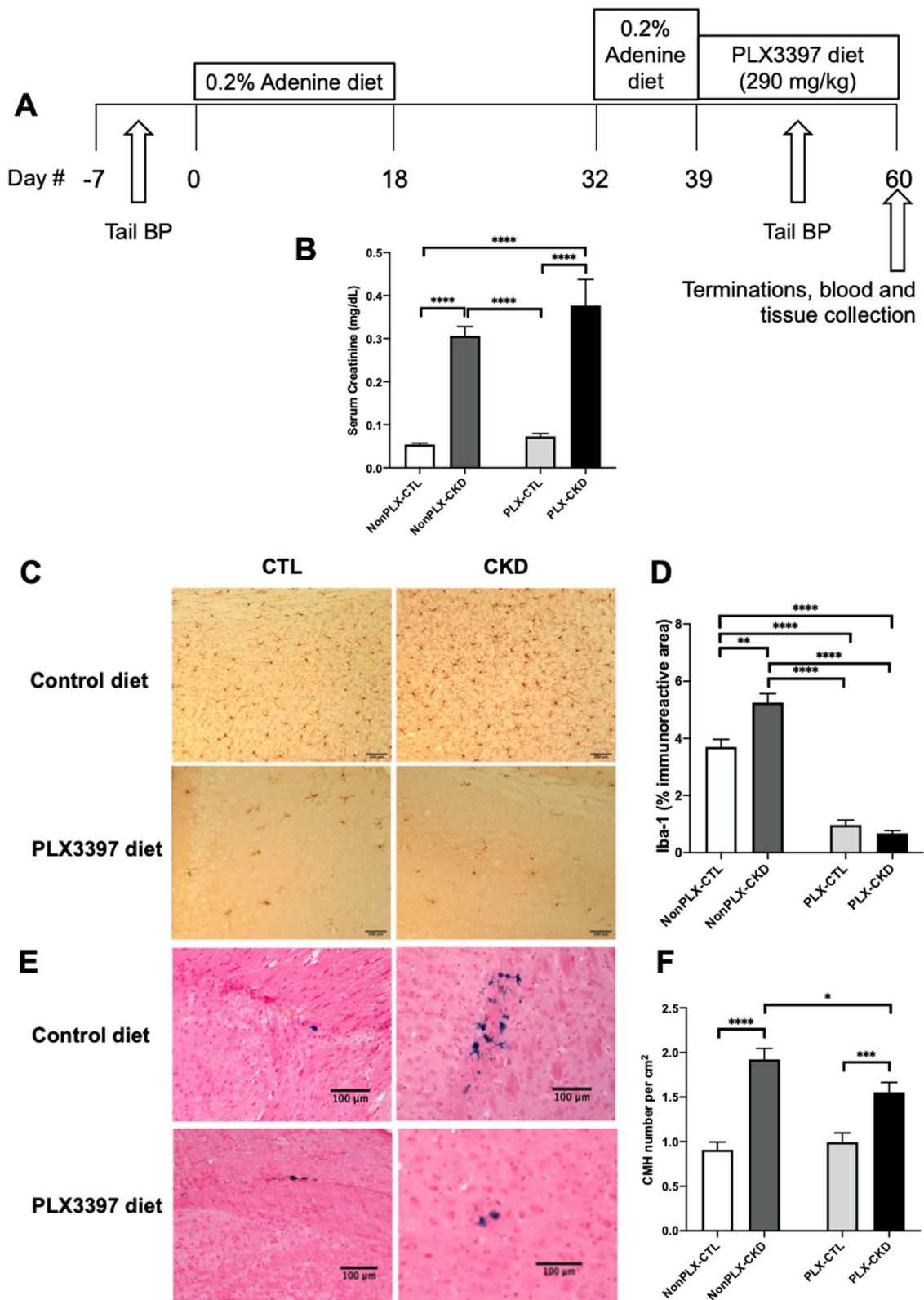


**Fig. 4** (See legend on previous page.)

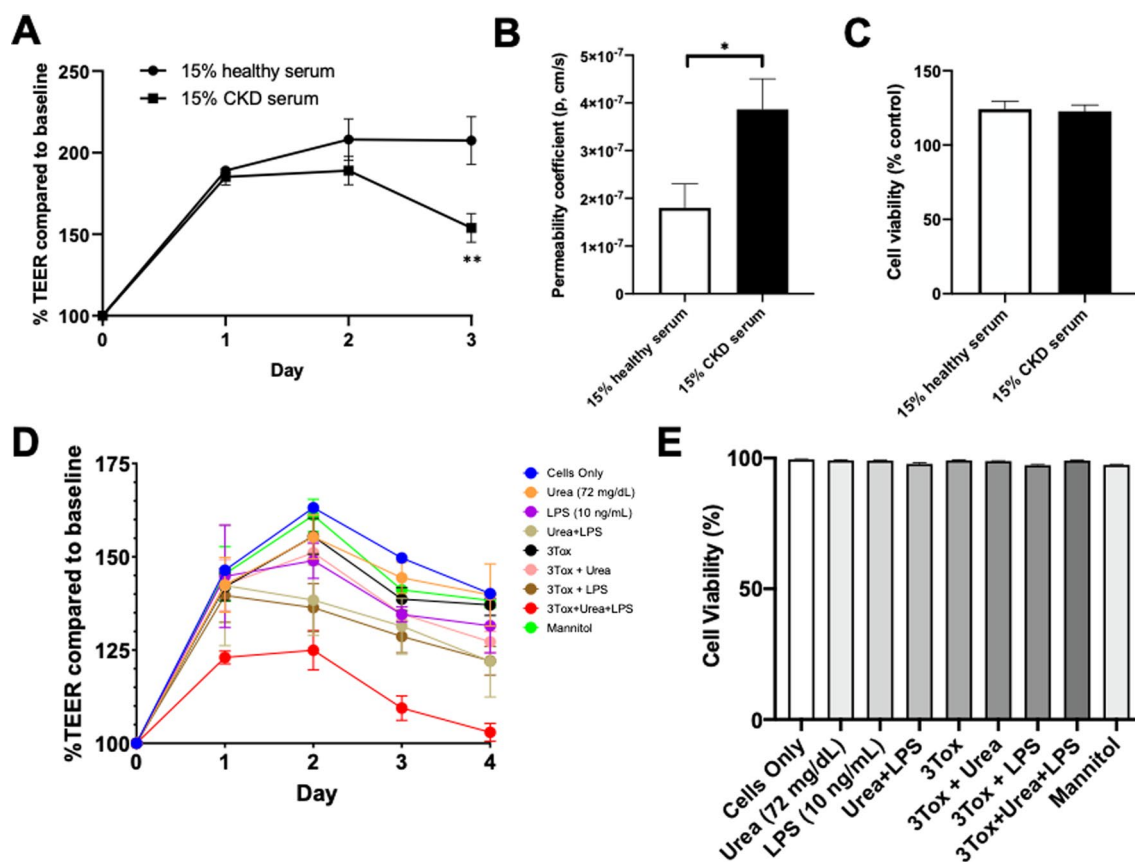


**Fig. 5** Serum-derived factors in CKD disrupted BBB integrity in vitro. **A–C** Effects of CKD dialysis serum on the iPSC-derived human brain microvascular endothelial cells (ihBMEC) monolayer. Incubation with CKD dialysis serum significantly decreased **A** TEER, and increased **B** tracer (sodium fluorescein) permeability across the ihBMEC monolayer 3 days after serum treatment initiation, compared with serum from healthy volunteers. **C** ihBMEC viability measured by CCK8 assay 3 days after serum treatment initiation was not changed. **D, E** Effects of uremic toxins on bEnd.3 endothelial barrier. **D** TEER remained significantly lower in the 3Tox + Urea + LPS group compared with the control group. After 4 days of toxin exposure, TEER was significantly lower in the Urea + LPS ( $p < 0.01$ ), 3Tox + LPS ( $p < 0.05$ ), and 3Tox + Urea + LPS group ( $p < 0.0001$ ) compared with the control group. **E** bEnd.3 cell viability was assessed by trypan blue assay and was equivalent across groups. 3Tox = indoxyl sulfate 150  $\mu\text{g}/\text{mL}$  + p-cresyl sulfate 100  $\mu\text{g}/\text{mL}$  + trimethylamine N-oxide 1  $\text{mg}/\text{mL}$ . The reference Cells Only group was cells grown in DMEM with 10% FBS, and mannitol 450  $\text{mg}/\text{dL}$  was used as an osmotic control group. Data shown are mean  $\pm$  SEM of at least 3 independent experiments done in duplicate. \* $p < 0.05$  and \*\* $p < 0.01$

faster CKD progression to end-stage renal disease and higher mortality in men than women [29–34]. While the underlying mechanisms are not completely understood, sex hormones are likely involved in CKD progression by mediating inflammation, oxidative stress, fibrosis, and activation of the renin–angiotensin system [35]. Testosterone exerts a deleterious effect in men by triggering apoptotic pathways leading to nephron cell loss and kidney structural damage [36]. By contrast, estrogen in women is renoprotective, attributable to the beneficial effects on vascular structure and function of endothelial and vascular smooth muscle cells [37]. Female sex hormone effects are less relevant in our study with aged mice; by age 17 months, 80% of female mice have irregular estrous cycles or have ceased cycling [38]. Regardless,

our findings have important implications that serum creatinine as a biomarker of kidney dysfunction also serves as a CMH risk marker.

CKD-induced neuroinflammation has been proposed as a key mechanism responsible for neurological dysfunction [39–41]. CKD progression contributed to increased production of pro-inflammatory cytokines and DNA damage in brain cells [40], increasing the likelihood of developing neurological dysfunction in patients with end-stage renal disease. Neuroinflammation is regulated by microglia and astrocytes, the innate immune cells of the central nervous system mediating the inflammatory response in aging, neurodegenerative disease, traumatic brain injury, and ischemic stroke [42–44]. Microglial dynamics are important in maintaining brain

homeostasis. Microglia are maintained in a resting state with a morphology characterized by long, ramified processes extending from the soma and terminating with bulbous endings; they can be activated when brain injuries are present, transforming into a phagocytic appearance, exhibiting large, rounded soma with no or few processes [25, 45]. Impaired microglial function has been implicated in aging [46] and Alzheimer's disease [47]. CKD-induced neuroinflammation has been associated with increased microglia/macrophage recruitment, a shift from an anti-inflammatory M2 to a pro-inflammatory M1 phenotype [48], and the formation of NLRP3 inflammasomes [49]. Although morphological profiles of microglia have been well-characterized in rodents [50], little is known about their morphological changes in the context of CKD, as well as the neuropathological consequences. In the current study, CKD is associated with microglial activation, shown by increased Iba-1 immunoreactivity and a phenotypic switch from resting to activated microglia (Fig. 3A–C).

We used Iba-1 immunostaining which identifies both microglia and macrophages [48]. We characterized the morphology of microglia at higher magnification (40x) to distinguish microglia from macrophages, which allowed us to determine the contribution of microglia in CKD-induced neuroinflammation (Fig. 3F). Our prior mouse work showed a positive correlation between Iba-1 immunoreactivity and CMH number [14]. Thus, the causal relationship between microglial activation and CMH formation was investigated in the current study using PLX3397 diet allowing for microglial depletion (Fig. 4). CKD-induced CMH formation was significantly decreased in aged mice with microglial depletion (Fig. 4F), while serum creatinine levels were found not to be affected (Fig. 4B). These findings indicate that CKD-induced CMH formation is at least partly mediated by microglial activation.

The BBB is formed by endothelial cells lining the capillary wall, astrocyte end-feet surrounding the capillary, and pericytes embedded in the baseline membrane, thus creating a physical barrier between the peripheral circulation and the central nervous system. The tight junctions between the endothelial cells serve to restrict passage of blood-borne substances (e.g., fibrinogen) into the brain and play a crucial role in brain homeostasis [51]. Impaired endothelial tight junctions at the BBB are well-characterized in aging brains [52] and can lead to passage of iron into the brain [53]. We have previously shown disruption in BBB tight junction proteins in young CKD mice during an inflammatory state [13]. Following the previous observations, we examined the passage of fibrinogen into the brains of CKD mice. Fibrinogen enters the brain after BBB injury and can be converted

into insoluble fibrin, contributing to neuroinflammation and neuronal damage in many conditions [54–57]. Fibrinogen/fibrin deposition is associated with microglial activation and increased immune cell recruitment into the brain [54, 58]. In line with this finding, we showed microglial activation and increased fibrinogen deposition in the brains of CKD mice (Fig. 3). Activated microglia modulate expression of tight junction proteins essential for BBB integrity [59], which may further exacerbate BBB disruption and CMH formation.

Our assessment of microvascular integrity *in vitro* has relied on TEER and tracer permeability measurements. TEER is the measurement of electrical resistance across a cellular monolayer to evaluate integrity of the endothelial monolayer. In our *in vitro* study with ihBMEC, TEER was elevated in the first 24 h due to the trophic factors present in the serum and reached the highest value at 48 h. Incubation with CKD serum caused injury to the monolayer, as shown by a reduction in TEER after serum treatment initiation (Fig. 5A). This is consistent with our previous findings from an *in vitro* study incubating mouse brain endothelial cells (bEnd.3) with CKD serum [13]. Furthermore, the decrease in TEER was accompanied by a two-fold increase in sodium fluorescein permeability across the ihBMEC monolayer (Fig. 5B). Sodium fluorescein is a small molecular weight tracer (MW: 376 Da) that more readily diffuses through the BBB than larger molecular weight tracers, and therefore has served as a common marker for altered permeability [26]. Previously, we showed an inverse correlation between sodium fluorescein permeability and TEER measurements across the ihBMEC monolayer [26]. Together, impairment of the monolayer induced by CKD-derived serum factors allows for increased passage of sodium fluorescein across the monolayer, suggesting disruption of the endothelial monolayer and consistent with BBB injury observed with fibrinogen immunostaining.

The murine gut microbiome changes with aging and is associated with alterations in microbial carbohydrate metabolism, decreased fecal short-chain fatty acids and decreased cobalamin and biotin biosynthesis [60, 61]. In the current study, we examined well-known gut-derived uremic toxins that are generated in the CKD milieu. These toxins are derived from amino acid catabolism by intestinal microbiota and are associated with systemic inflammation and vascular injury in CKD [62–65]. The exact uremic toxins that contribute to BBB disruption and whether the effects are results of an individual toxin or a combination of several toxins remain largely unknown. We have previously shown CKD serum from dialysis patients caused marked drop in TEER, and urea was one of the key uremic toxins. Exposure of bEnd.3 cells to urea at concentrations approximate to the values

measured in dialysis patients reduced TEER in a dose-dependent manner [13]. In the current *in vitro* study, this was further investigated by exposing bEnd.3 mouse brain endothelial cells with various gut-derived uremic toxins alone and in combination, with TEER measurements every 24 h. We demonstrated that uremic toxins (i.e., IS, PCS, and TMAO) in combination with urea and LPS exerted the most deleterious effects on the endothelial barrier. TEER was significantly lower in the 3Toxins+Urea+LPS group compared with the control group, and eventually declined to a level close to the baseline values at day 4 (Fig. 5D). These findings suggest gut-derived uremic toxins aggravate urea/LPS-induced bEnd.3 endothelial barrier dysfunction, again consistent with findings of BBB injury observed with fibrinogen immunostaining.

Despite these multiple findings, this study has some limitations. The mouse study suggests a key role of microglia in mediating CMH formation in CKD animals. It should be noted that the use of CSF1R inhibitor PLX3397 eliminates microglia in the parenchyma, but also affects the number of non-parenchymal macrophages in the perivascular spaces, the choroid plexus, and the meninges [66], which are known to cause neurovascular dysfunction [67]. Our findings do not rule-out a contribution of perivascular macrophages to CMH formation [68], a subject that warrants further investigation. The binary morphological categorization of microglia into resting and activated states may be an oversimplification. Microglia intermediate between the two states may adopt various functions in immune cell recruitment and activation, cell proliferation, and phagocytosis as their morphology changes [69]. Note that the vascular source of CMH in uremic milieu remains unclear, as iron uptake into the brain is highly regulated by BBB. Mouse models and human postmortem studies of aging, hypertension, and Alzheimer's disease have suggested a capillary source of CMH involving BBB disruption [14, 70–72], consistent with the findings from the *in vitro* CKD models we investigated. However, these findings should be interpreted with caution, because CMH may develop via a mechanism independent of capillary injury [73–75]. To expand our knowledge on the vascular source of CMH, we have developed a semi-automated approach to characterize microvascular network in three-dimensional (3D) imaging of mouse brains [76]; this will enable us to visualize the co-localization of fluorescently labeled microvascular network and Prussian blue-positive CMH and therefore, identify the vascular origin of CMH. In addition, the issue of cognitive decline with CKD is important, as we have emphasized [77]. However, the experiments in our manuscript were neither designed nor powered to address

this issue. In terms of *in vitro* BBB models, recent studies show that ihBMEC have a mixed endothelial–epithelial transcriptional profile [26, 78, 79], and we therefore used two different brain endothelial cell culture systems, i.e., ihBMEC and bEnd.3 cells, for a better understanding of the mechanistic role of microvascular endothelial function in CKD-induced CMH formation.

## Conclusions

Adenine-induced CKD promotes the development of CMH in aged C57BL/6J mice independent of blood pressure, likely via microglial activation and BBB disruption. Extent of CMH development is directly proportional to degree of renal insufficiency. Moreover, serum-derived factors in CKD disrupt endothelial monolayer by reducing TEER and enhancing the passage of sodium fluorescein across the monolayer. Gut-derived uremic toxins (i.e., IS, PCS, and TMAO) aggravated urea/LPS-induced endothelial barrier dysfunction by producing a marked drop in TEER, supporting the key role of uremic toxins in CKD-specific mechanisms that contribute to microvascular dysfunction. These findings indicate that CKD provokes microvascular injury leading to CMH formation in this model and suggest that CKD makes an important contribution to cerebral small vessel disease.

## Abbreviations

|                |  |
|----------------|--|
| ABC            | Avidin–biotin-peroxidase                                     |
| BBB            | Blood–brain barrier  |
| bFGF           | Basic fibroblast growth factor                               |
| CCK-8          | Cell Counting Kit-8  |
| CKD            | Chronic kidney disease                                       |
| CMH            | Cerebral microhemorrhages                                    |
| CSF1R          | Colony-stimulating factor 1 receptor                         |
| DAB            | 3,3'-Diaminobenzidine  |
| DMEM           | Dulbecco's Modified Eagle's Medium                           |
| DMEM/Ham's F12 | Dulbecco's Modified Eagle Medium/Ham's nutrient mixture F-12 |
| FBS            | Fetal bovine serum   |
| GFAP           | Glial fibrillary acidic protein                              |
| hESFM          | Human endothelial serum-free medium                          |
| ihBMEC         | Human brain microvascular endothelial cells                  |
| IMR90-4        | IMR90 clone 4 line   |
| iPSC           | Human induced pluripotent stem cell                          |
| IS             | Indoxyl sulfate  |
| LC–MS/MS       | Liquid chromatography with tandem mass spectrometry          |
| LDL            | Low-density lipoprotein                                      |
| LPS            | Lipopolysaccharide   |
| MEM–NEAA       | Minimum essential medium–nonessential amino acids            |
| PBS            | Phosphate-buffered saline                                    |
| PCS            | P-cresyl sulfate   |
| ROCK           | Rho-associated protein kinase                                |
| RT             | Room temperature   |
| TEER           | Transendothelial electrical resistance                       |
| TMAO           | Trimethylamine-N-oxide                                       |
| WWF            | Von Willebrand factor  |

**Acknowledgements**

Not applicable.

**Author contributions**

CF, WLL, JS, RC, APH, RKS, DHC, and MF designed the study, analyzed the results, and wrote and revised the manuscript. CF, JS, RC, JL, and HL performed the experiments and collected data. CF, JS, RC, AV, DL, YHH and YZ participated in the data acquisition, analysis, and interpretation. All authors read and approved the final manuscript.

**Funding**

Research reported in this publication was supported by the National Institute of Neurological Disorders and Stroke under award numbers R01NS20989 (MJF and DHC), R01NS113337 (WLL), and by the National Institute of Aging under award numbers R01AG072896 and R01AG062840 (RKS) of the National Institutes of Health. Approximately \$400K (100%) of Federal funds supported this project. The content is solely the responsibility of the authors and does not necessarily represent the official views of the National Institutes of Health.

**Availability of data and materials**

Data are available upon reasonable request.

**Declarations****Ethics approval and consent to participate**

All experimental procedures described in this article were approved the Institutional Animal Care and Use Committee or Institutional Review Board at the University of California, Irvine.

**Consent for publication**

Not applicable.

**Competing interests**

The authors declare that they have no competing interests.

**Author details**

<sup>1</sup>Department of Neurology, University of California, Irvine, CA, USA. <sup>2</sup>Department of Medicine, Division of Nephrology, University of California, Irvine, CA, USA. <sup>3</sup>Department of Biomedical and Pharmaceutical Sciences, School of Pharmacy, Chapman University, Irvine, CA, USA. <sup>4</sup>Institute for Memory Impairments and Neurological Disorders, University of California, Irvine, CA, USA. <sup>5</sup>Department of Pathology & Laboratory Medicine, University of California, Irvine, CA, USA. <sup>6</sup>Department of Neurology, UC Irvine Medical Center, 101 The City Drive South, Shanbrom Hall (Building 55), Room 121, Orange, CA 92868, USA.

Received: 26 September 2022 Accepted: 20 January 2023

Published online: 25 February 2023

**References**

- Centers for disease control and prevention. Chronic kidney disease in the United States 2021. Atlanta: US Department of Health and Human Services, Centers for Disease Control and Prevention; 2021.
- Etgen T, Chonchol M, Förstl H, Sander D. Chronic kidney disease and cognitive impairment: a systematic review and meta-analysis. *Am J Nephrol.* 2012;35:474–82.
- Masson P, Kelly PJ, Craig JC, Lindley RI, Webster AC. Risk of stroke in patients with ESRD. *Clin J Am Soc Nephrol.* 2015;10:1585–92.
- Vanent KN, Leasure AC, Acosta JN, Kuohn LR, Woo D, Murthy SB, Kamel H, Messé SR, Mullen MT, Cohen JB, et al. Association of chronic kidney disease with risk of intracerebral hemorrhage. *JAMA Neurol.* 2022;79:911–8.
- Chiu YL, Tsai HH, Lai YJ, Tseng HY, Wu YW, Peng YS, Chiu CM, Chuang YF. Cognitive impairment in patients with end-stage renal disease: accelerated brain aging? *J Formos Med Assoc.* 2019;118:867–75.
- Donkor ES. Stroke in the 21(st) century: a snapshot of the burden, epidemiology, and quality of life. *Stroke Res Treat.* 2018;2018:3238165.
- Vinters HV, Magaki SD, Williams CK. Neuropathologic findings in chronic kidney disease (CKD). *J Stroke Cerebrovasc Dis.* 2021;30: 105657.
- Lau WL, Huisa BN, Fisher M. The cerebrovascular-chronic kidney disease connection: perspectives and mechanisms. *Transl Stroke Res.* 2017;8:67–76.
- Poels MM, Vernooij MW, Ikram MA, Hofman A, Krestin GP, van der Lugt A, Breteler MM. Prevalence and risk factors of cerebral microbleeds: an update of the Rotterdam scan study. *Stroke.* 2010;41:S103–106.
- Chai C, Wang Z, Fan L, Zhang M, Chu Z, Zuo C, Liu L, Mark Haacke E, Guo W, Shen W, Xia S. Increased number and distribution of cerebral microbleeds is a risk factor for cognitive dysfunction in hemodialysis patients: a longitudinal study. *Medicine.* 2016;95: e2974.
- Ovbiagele B, Wing JJ, Menon RS, Burgess RE, Gibbons MC, Sobotka I, German L, Shara NM, Fernandez S, Jayam-Trouth A, et al. Association of chronic kidney disease with cerebral microbleeds in patients with primary intracerebral hemorrhage. *Stroke.* 2013;44:2409–13.
- Shima H, Mori T, Ooi M, Sonoda M, Shoji T, Ishimura E, Okamura M, Ishizaka N, Inaba M. Silent cerebral microbleeds and longitudinal risk of renal and cardiovascular events in patients with CKD. *Clin J Am Soc Nephrol.* 2016;11:1557–65.
- Lau WL, Nunes ACF, Vasilevko V, Floriolli D, Lertpanit L, Savoij J, Bangash M, Yao Z, Shah K, Naqvi S, et al. Chronic kidney disease increases cerebral microbleeds in mouse and man. *Transl Stroke Res.* 2020;11:122–34.
- Sumbria RK, Grigoryan MM, Vasilevko V, Paganini-Hill A, Kilday K, Kim R, Cribbs DH, Fisher MJ. Aging exacerbates development of cerebral microbleeds in a mouse model. *J Neuroinflammation.* 2018;15:69.
- Figuer A, Bodega G, Tato P, Valera G, Serroukh N, Ceprian N, de Sequera P, Morales E, Carracedo J, Ramírez R, Alique M. Premature aging in chronic kidney disease: the outcome of persistent inflammation beyond the bounds. *Int J Environ Res Public Health.* 2021;18:8044.
- Xu KY, Xia GH, Lu JQ, Chen MX, Zhen X, Wang S, You C, Nie J, Zhou HW, Yin J. Impaired renal function and dysbiosis of gut microbiota contribute to increased trimethylamine-N-oxide in chronic kidney disease patients. *Sci Rep.* 2017;7:1445.
- McIntyre CW, Harrison LE, Eldehni MT, Jefferies HJ, Szeto CC, John SG, Sigrist MK, Burton JO, Hothi D, Korsheed S, et al. Circulating endotoxemia: a novel factor in systemic inflammation and cardiovascular disease in chronic kidney disease. *Clin J Am Soc Nephrol.* 2011;6:133–41.
- Duranton F, Cohen G, De Smet R, Rodriguez M, Jankowski J, Vanholder R, Argiles A. Normal and pathologic concentrations of uremic toxins. *J Am Soc Nephrol.* 2012;23:1258–70.
- Assem M, Lando M, Grissi M, Kamel S, Massy ZA, Chillon JM, Hénaut L. The impact of uremic toxins on cerebrovascular and cognitive disorders. *Toxins.* 2018;10:303.
- Fox JG, Barthold S, Davisson M, Newcomer CE, Quimby FW, Smith A. The mouse in biomedical research: normative biology, husbandry, and models. Amsterdam: Elsevier; 2006.
- Passos GF, Kilday K, Gillen DL, Cribbs DH, Vasilevko V. Experimental hypertension increases spontaneous intracerebral hemorrhages in a mouse model of cerebral amyloidosis. *J Cereb Blood Flow Metab.* 2016;36:399–404.
- Elmore MR, Najafi AR, Koike MA, Dagher NN, Spangenberg EE, Rice RA, Kitazawa M, Matusow B, Nguyen H, West BL, Green KN. Colony-stimulating factor 1 receptor signaling is necessary for microglia viability, unmasking a microglia progenitor cell in the adult brain. *Neuron.* 2014;82:380–97.
- Kennedy DJ, Vetteth S, Periyasamy SM, Kanj M, Fedorova L, Khouri S, Kahaleh MB, Xie Z, Malhotra D, Kolodkin NI, et al. Central role for the cardiotoxic steroid marinobufagenin in the pathogenesis of experimental uremic cardiomyopathy. *Hypertension.* 2006;47:488–95.
- Lau WL, Khazaeli M, Savoij J, Manekia K, Bangash M, Thakurta RG, Dang A, Vaziri ND, Singh B. Dietary tetrahydrocurcumin reduces renal fibrosis and cardiac hypertrophy in 5/6 nephrectomized rats. *Pharmacol Res Perspect.* 2018;6: e00385.
- Crews FT, Vetreño RP. Mechanisms of neuroimmune gene induction in alcoholism. *Psychopharmacology.* 2016;233:1543–57.
- Sun J, Ou W, Han D, Paganini-Hill A, Fisher MJ, Sumbria RK. Comparative studies between the murine immortalized brain endothelial cell line (bEnd.3) and induced pluripotent stem cell-derived human brain endothelial cells for paracellular transport. *PLoS ONE.* 2020;17: e0268860.
- Rodrigues WF, Miguel CB, Napimoga MH, Oliveira CJ, Lazo-Chica JE. Establishing standards for studying renal function in mice through

- measurements of body size-adjusted creatinine and urea levels. *Biomed Res Int.* 2014;2014: 872827.
28. Keane L, Antignano I, Riechers SP, Zollinger R, Dumas AA, Offermann N, Bernis ME, Russ J, Graelmann F, McCormick PN, et al. mTOR-dependent translation amplifies microglia priming in aging mice. *J Clin Invest.* 2021. <https://doi.org/10.1172/JCI155208>.
  29. Neugartern J, Acharya A, Silbiger SR. Effect of gender on the progression of nondiabetic renal disease: a meta-analysis. *J Am Soc Nephrol.* 2000;11:319–29.
  30. Hecking M, Bieber BA, Ethier J, Kautzky-Willer A, Sunder-Plassmann G, Säemann MD, Ramirez SP, Gillespie BW, Pisoni RL, Robinson BM, Port FK. Sex-specific differences in hemodialysis prevalence and practices and the male-to-female mortality rate: the dialysis outcomes and practice patterns study (DOPPS). *PLoS Med.* 2014;11: e1001750.
  31. Ricardo AC, Yang W, Sha D, Appel LJ, Chen J, Krousel-Wood M, Manoharan A, Steigerwalt S, Wright J, Rahman M, et al. Sex-related disparities in CKD progression. *J Am Soc Nephrol.* 2019;30:137–46.
  32. Minutolo R, Gabbai FB, Chiodini P, Provenzano M, Borrelli S, Garofalo C, Bellizzi V, Russo D, Conte G, De Nicola L. Sex differences in the progression of CKD among older patients: pooled analysis of 4 cohort studies. *Am J Kidney Dis.* 2020;75:30–8.
  33. Antlanger M, Noordzij M, van de Luitgaarden M, Carrero JJ, Palsson R, Finne P, Hemmeler MH, Aresté-Fosalba N, Reisaeter AV, Cases A, et al. Sex differences in kidney replacement therapy initiation and maintenance. *Clin J Am Soc Nephrol.* 2019;14:1616–25.
  34. Hödlmoser S, Winkelmayer WC, Zee J, Pecoits-Filho R, Pisoni RL, Port FK, Robinson BM, Ristl R, Krenn S, Kurnikowski A, et al. Sex differences in chronic kidney disease awareness among US adults, 1999 to 2018. *PLoS ONE.* 2020;15: e0243431.
  35. Valdivielso JM, Jacobs-Cachá C, Soler MJ. Sex hormones and their influence on chronic kidney disease. *Curr Opin Nephrol Hypertens.* 2019;28:1–9.
  36. Verzola D, Gandolfo MT, Salvatore F, Villaggio B, Gianiorio F, Traverso P, Deferrari G, Garibotto G. Testosterone promotes apoptotic damage in human renal tubular cells. *Kidney Int.* 2004;65:1252–61.
  37. Usselman CW, Stachenfeld NS, Bender JR. The molecular actions of oestrogen in the regulation of vascular health. *Exp Physiol.* 2016;101:356–61.
  38. Frick KM, Burlingame LA, Arters JA, Berger-Sweeney J. Reference memory, anxiety and estrous cyclicity in C57BL/6NIA mice are affected by age and sex. *Neuroscience.* 2000;95:293–307.
  39. Mazumder MK, Paul R, Bhattacharya P, Borah A. Neurological sequel of chronic kidney disease: from diminished Acetylcholinesterase activity to mitochondrial dysfunctions, oxidative stress and inflammation in mice brain. *Sci Rep.* 2019;9:3097.
  40. Hirotsu C, Tufik S, Ribeiro DA, Alvarenga TA, Andersen ML. Genomic damage in the progression of chronic kidney disease in rats. *Brain Behav Immun.* 2011;25:416–22.
  41. Jin WS, Shen LL, Bu XL, Zhang WW, Chen SH, Huang ZL, Xiong JX, Gao CY, Dong Z, He YN, et al. Peritoneal dialysis reduces amyloid-beta plasma levels in humans and attenuates Alzheimer-associated phenotypes in an APP/PS1 mouse model. *Acta Neuropathol.* 2017;134:207–20.
  42. Mayne K, White JA, McMurrin CE, Rivera FJ, de la Fuente AG. Aging and neurodegenerative disease: is the adaptive immune system a friend or foe? *Front Aging Neurosci.* 2020;12: 572090.
  43. Xue Y, Nie D, Wang LJ, Qiu HC, Ma L, Dong MX, Tu WJ, Zhao J. Microglial polarization: novel therapeutic strategy against ischemic stroke. *Aging Dis.* 2021;12:466–79.
  44. Singh D. Astrocytic and microglial cells as the modulators of neuroinflammation in Alzheimer's disease. *J Neuroinflammation.* 2022;19:206.
  45. Colonna M, Butovsky O. Microglia function in the central nervous system during health and neurodegeneration. *Annu Rev Immunol.* 2017;35:441–68.
  46. Niraula A, Sheridan JF, Godbout JP. Microglia priming with aging and stress. *Neuropsychopharmacology.* 2017;42:318–33.
  47. Angelova DM, Brown DR. Microglia and the aging brain: are senescent microglia the key to neurodegeneration? *J Neurochem.* 2019;151:676–88.
  48. Hénaut L, Grissi M, Brazier F, Assem M, Poirot-Leclercq S, Lenglet G, Boudot C, Avondo C, Boullier A, Choukroun G, et al. Cellular and molecular mechanisms associated with ischemic stroke severity in female mice with chronic kidney disease. *Sci Rep.* 2019;9:6432.
  49. Li LC, Chen WY, Chen JB, Lee WC, Chang CC, Tzeng HT, Huang CC, Chang YJ, Yang JL. The AST-120 recovers uremic toxin-induced cognitive deficit via NLRP3 inflammasome pathway in astrocytes and microglia. *Biomedicines.* 2021;9:1252.
  50. Savage JC, Carrier M, Tremblay M-È. Morphology of microglia across contexts of health and disease. In: Verkhratsky A, Garaschuk O, editors. *Microglia: methods and protocols.* New York: Springer; 2019.
  51. Abbott NJ, Patabendige AA, Dolman DE, Yusof SR, Begley DJ. Structure and function of the blood-brain barrier. *Neurobiol Dis.* 2010;37:13–25.
  52. Elahy M, Jackaman C, Mamo JC, Lam V, Dhaliwal SS, Giles C, Nelson D, Takechi R. Blood-brain barrier dysfunction developed during normal aging is associated with inflammation and loss of tight junctions but not with leukocyte recruitment. *Immun Ageing.* 2015;12:2.
  53. Zhao Y, Liu Y, Xu Y, Li K, Zhou L, Qiao H, Xu Q, Zhao J. The role of ferroptosis in blood-brain barrier injury. *Cell Mol Neurobiol.* 2022. <https://doi.org/10.1007/s10571-022-01197-5>.
  54. Davalos D, Ryu JK, Merlini M, Baeten KM, Le Moan N, Petersen MA, Deerinck TJ, Smirnov DS, Bedard C, Hakozaki H, et al. Fibrinogen-induced perivascular microglial clustering is required for the development of axonal damage in neuroinflammation. *Nat Commun.* 2012;3:1227.
  55. Paul J, Strickland S, Melchor JP. Fibrin deposition accelerates neurovascular damage and neuroinflammation in mouse models of Alzheimer's disease. *J Exp Med.* 2007;204:1999–2008.
  56. Cortes-Canteli M, Paul J, Norris EH, Bronstein R, Ahn HJ, Zamolodchikov D, Bhuvanendran S, Fenz KM, Strickland S. Fibrinogen and beta-amyloid association alters thrombosis and fibrinolysis: a possible contributing factor to Alzheimer's disease. *Neuron.* 2010;66:695–709.
  57. Schachtrup C, Ryu JK, Helmrick MJ, Vagena E, Galanakis DK, Degen JL, Margolis RU, Akassoglou K. Fibrinogen triggers astrocyte scar formation by promoting the availability of active TGF-beta after vascular damage. *J Neurosci.* 2010;30:5843–54.
  58. Ryu JK, Petersen MA, Murray SG, Baeten KM, Meyer-Franke A, Chan JP, Vagena E, Bedard C, Machado MR, Rios Coronado PE, et al. Blood coagulation protein fibrinogen promotes autoimmunity and demyelination via chemokine release and antigen presentation. *Nat Commun.* 2015;6:8164.
  59. Rochford KD, Collins LE, Murphy RP, Cummins PM. Downregulation of blood-brain barrier phenotype by proinflammatory cytokines involves NADPH oxidase-dependent ROS generation: consequences for interendothelial adherens and tight junctions. *PLoS ONE.* 2014;9: e101815.
  60. Langille MG, Meehan CJ, Koenig JE, Dhanani AS, Rose RA, Howlett SE, Beiko RG. Microbial shifts in the aging mouse gut. *Microbiome.* 2014;2:50.
  61. You X, Dadwal UC, Lenburg ME, Kacena MA, Charles JF. Murine gut microbiome meta-analysis reveals alterations in carbohydrate metabolism in response to aging. *GmSystems.* 2022;7: e0124821.
  62. Vaziri ND, Wong J, Pahl M, Piceno YM, Yuan J, Desantis TZ, Ni Z, Nguyen TH, Andersen GL. Chronic kidney disease alters intestinal microbial flora. *Kidney Int.* 2013;83:308–15.
  63. Mishima E, Fukuda S, Mukawa C, Yuri A, Kanemitsu Y, Matsumoto Y, Akiyama Y, Fukuda NN, Tsukamoto H, Asaji K, et al. Evaluation of the impact of gut microbiota on uremic solute accumulation by a CE-TOFMS-based metabolomics approach. *Kidney Int.* 2017;92:634–45.
  64. Lau WL, Savoj J, Nakata MB, Vaziri ND. Altered microbiome in chronic kidney disease: systemic effects of gut-derived uremic toxins. *Clin Sci (Lond).* 2018;132:509–22.
  65. Yang T, Richards EM, Pepine CJ, Raizada MK. The gut microbiota and the brain-gut-kidney axis in hypertension and chronic kidney disease. *Nat Rev Nephrol.* 2018;14:442–56.
  66. Mildenerberger W, Stifter SA, Greter M. Diversity and function of brain-associated macrophages. *Curr Opin Immunol.* 2022;76: 102181.
  67. Santisteban MM, Ahn SJ, Lane D, Faraco G, Garcia-Bonilla L, Racchumi G, Poon C, Schaeffer S, Segarra SG, Körbelin J, et al. Endothelium-macrophage crosstalk mediates blood-brain barrier dysfunction in hypertension. *Hypertension.* 2020;76:795–807.
  68. Polfitt MM, Goede PH, van Kesteren-Hendriks EM, van Rooijen N, Dijkstra CD, van den Berg TK. A method for the selective depletion of perivascular and meningeal macrophages in the central nervous system. *J Neuroimmunol.* 2001;116:188–95.
  69. Karperien A, Ahammer H, Jelinek HF. Quantitating the subtleties of microglial morphology with fractal analysis. *Front Cell Neurosci.* 2013;7:3.
  70. Fisher M, French S, Ji P, Kim RC. Cerebral microbleeds in the elderly: a pathological analysis. *Stroke.* 2010;41:2782–5.

71. Craggs LJ, Yamamoto Y, Deramecourt V, Kalaria RN. Microvascular pathology and morphometrics of sporadic and hereditary small vessel diseases of the brain. *Brain Pathol.* 2014;24:495–509.
72. Kalaria RN. Cerebrovascular degeneration is related to amyloid-beta protein deposition in Alzheimer's disease. *Ann NY Acad Sci.* 1997;826:263–71.
73. Chang R, Castillo J, Zambon AC, Krasieva TB, Fisher MJ, Sumbria RK. Brain endothelial erythrophagocytosis and hemoglobin transmigration across brain endothelium: implications for pathogenesis of cerebral microbleeds. *Front Cell Neurosci.* 2018;12:279.
74. Wadi LC, Grigoryan MM, Kim RC, Fang C, Kim J, Corrada MM, Paganini-Hill A, Fisher MJ. Mechanisms of cerebral microbleeds. *J Neuropathol Exp Neurol.* 2020;79:1093–9.
75. Shih AY, Hyacinth HI, Hartmann DA, van Veluw SJ. Rodent models of cerebral microinfarct and microhemorrhage. *Stroke.* 2018;49:803–10.
76. Xie DF, Crouzet C, Lopresti K, Wang Y, Robinson C, Jones W, Muqolli F, Pai A, Fang C, Cribbs DH. Semi-automated protocol to quantify and characterize fluorescent, 3D vascular images. *bioRxiv.* 2022. <https://doi.org/10.1101/2022.05.05.490827>.
77. Lau WL, Fisher M. New insights into cognitive decline in chronic kidney disease. *Nat Rev Nephrol.* 2022. <https://doi.org/10.1038/s41581-022-00656-y>.
78. Delsing L, Dönnnes P, Sánchez J, Clausen M, Voulgaris D, Falk A, Herland A, Brölén G, Zetterberg H, Hicks R, Synnergren J. Barrier properties and transcriptome expression in human iPSC-derived models of the blood-brain barrier. *Stem Cells.* 2018;36:1816–27.
79. Lu TM, Houghton S, Magdeldin T, Durán JGB, Minotti AP, Snead A, Sproul A, Nguyen D-HT, Xiang J, Fine HA, et al. Pluripotent stem cell-derived epithelium misidentified as brain microvascular endothelium requires ETS factors to acquire vascular fate. *Proc Natl Acad Sci.* 2021;118: e2016950118.

## Publisher's Note

Springer Nature remains neutral with regard to jurisdictional claims in published maps and institutional affiliations.

Ready to submit your research? Choose BMC and benefit from:

- fast, convenient online submission
- thorough peer review by experienced researchers in your field
- rapid publication on acceptance
- support for research data, including large and complex data types
- gold Open Access which fosters wider collaboration and increased citations
- maximum visibility for your research: over 100M website views per year

At BMC, research is always in progress.

Learn more [biomedcentral.com/submissions](https://biomedcentral.com/submissions)

